ADVANCES IN ATMOSPHERIC SCIENCES, VOL. 31, MAY 2014, 525–531

Effects of Doubled Carbon Dioxide on Rainfall Responses to Large-Scale Forcing: A Two-Dimensional Cloud-Resolving Modeling Study

LI Xiaofan*[1], SHEN Xinyong[2], and LIU Jia[2]

[1]*Department of Earth Sciences, Zhejiang University, Hangzhou* 310027
[2]*Key Laboratory of Meteorological Disaster of the Ministry of Education, Nanjing University of Information Science and Technology, Nanjing* 210044

(Received 4 February 2013; revised 3 July 2013; accepted 9 September 2013)

ABSTRACT

Rainfall responses to doubled atmospheric carbon dioxide concentration were investigated through the analysis of two pairs of two-dimensional cloud-resolving model sensitivity experiments. One pair of experiments simulated pre-summer heavy rainfall over southern China around the summer solstice, whereas the other pair of experiments simulated tropical rainfall around the winter solstice. The analysis of the time and model domain mean heat budget revealed that the enhanced local atmospheric warming was associated with doubled carbon dioxide through the weakened infrared radiative cooling during the summer solstice. The weakened mean pre-summer rainfall corresponded to the weakened mean infrared radiative cooling. Doubled carbon dioxide increased the mean tropical atmospheric warming via the enhanced mean latent heat in correspondence with the strengthened mean infrared radiative cooling during the winter solstice. The enhanced mean tropical rainfall was associated with the increased mean latent heat.

Key words: doubled carbon dioxide, radiation, latent heat, condensation, rainfall, cloud-resolving model simulation

Citation: Li, X. F., X. Y. Shen, and J. Liu, 2014: Effects of doubled carbon dioxide on rainfall responses to large-scale forcing: A two-dimensional cloud-resolving modeling study. *Adv. Atmos. Sci.*, **31**(3), 525–531, doi: 10.1007/s00376-013-3030-2.

1. Introduction

The increase in tropospheric temperature in recent centuries may be associated with the increase in greenhouse gases (IPCC, 2001, 2007). The steady increase of greenhouse gases in the global atmosphere caused by human activities, such as burning fossil fuels, may lead to the increase in surface temperature (Manabe and Wetherald, 1975; Folland et al., 2001; Jones and Moberg, 2003) and precipitation (Fields et al., 1993; Li et al., 2011). The increase in greenhouse gases also causes changes in atmospheric circulations (Chen and Held, 2007; Vecchi and Soden, 2007; Wu et al., 2012), the hydrological cycle (Manabe and Wetherald, 1975), and ecology (Bazzaz, 1990). Numerical modeling has shown that the increase in regional-scale (Meehl et al., 2005; Tebaldi et al., 2006) and global-scale (Emori and Brown, 2005; Kharin and Zwiers, 2005) precipitation extremes may be related to the warmer climate caused by the increase in greenhouse gases. Since previous numerical studies focused on the relationship between precipitation and doubled atmospheric carbon dioxide at the climate timescale, the dominant water vapor, cloud, and heat processes that are responsible for the effects of doubled carbon dioxide on precipitation have seldom been studied. What are the effects of increased carbon dioxide on rainfall? Under the condition of doubled carbon dioxide, what are the rainfall responses and associated changes in the thermal budget? What are the major physical processes that are responsible for the responses of rainfall, heat, and water vapor to the increased carbon dioxide? Due to their coarse horizontal resolution, large-scale circulation models usually use diagnostic cloud parameterization schemes. Cloud microphysical processes are directly responsible for the production of precipitation. Doubled carbon dioxide changes the radiation and associated thermal stratification through cloud-radiation interaction processes. Thus, a cloud-resolving model with prognostic cloud microphysical schemes is required to study the effects of doubled carbon dioxide on rainfall.

To answer these questions, a series of sensitivity experiments were carried out in this study. Since the change in carbon dioxide may lead to a change in solar heating and the solar heating rates around the summer and winter solstices could have the largest differences, the pre-summer heavy rainfall event that occurred around the summer solstice and the tropical rainfall event during the Tropical Ocean Global

* Corresponding author: LI Xiaofan
Email: xiaofanli@zju.edu.cn

Atmosphere–Coupled Ocean Atmosphere Response Experiment (TOGA COARE) that occurred around the winter solstice were chosen for this study. In this study, precipitation responses to doubled atmospheric carbon dioxide concentration are investigated through the partitioning analysis of two pairs of sensitivity experiments. The sensitivity experiments were conducted using a two-dimensional cloud-resolving model. The designs of the control and sensitivity experiments, and the heat and surface rainfall budgets are briefly described in section 2. The results are presented in section 3. A summary is given in section 4.

2. Experiments and analysis methodologies

The pre-summer rainfall control experiment (PSR) was simulated from 0200 LST 3 June to 0200 LST 8 June 2008, whereas the tropical rainfall control experiment (COARE) was simulated from 1000 LST 19 December to 1000 LST 24 December 1992. The large-scale forcing included vertical velocity and zonal wind in both cases. The vertical velocity and wind were averaged over a longitudinally oriented rectangular area of (21°–22°N, 108°–116°E) using the Global Data Assimilation System (GDAS) developed by National Centers for Environmental Prediction (NCEP), National Oceanic and Atmospheric Administration (NOAA), USA in the PSR case, whereas in the COARE case they were obtained from the observational data over the Intensive Flux Array (IFA) during the TOGA COARE. The hourly SST at the Improved Meteorological (IMET) surface mooring buoy (1.75°S, 156°E) (Weller and Anderson, 1996) was imposed in the COARE case. The surface fluxes calculated from the GDAS data were imposed in the PSR case. The cloud-resolving model simulations have been validated with rain gauge observation and temperature and specific humidity data in the PSR case (Wang et al., 2010; Shen et al., 2011b) and with rain rate, temperature, specific humidity, and surface solar radiation and latent heat fluxes in the COARE case (Li et al., 1999). The PSR and associated sensitivity experiments have been used to study the effects of vertical wind shear and cloud radiative processes (Shen et al., 2011b) and ice (Wang et al., 2010; Shen et al., 2011c) and water clouds on pre-summer rainfall (Shen et al., 2011a). The COARE and associated sensitivity experiments have been used to study radiative and microphysical effects on the improvement of thermodynamic simulations (Li et al., 1999), phase difference between energy and rainfall (Li et al., 2002a), and dominant microphysical processes (Li et al. 2002b).

The model used in Shen et al. (2011b) and Li et al. (1999) and this study is the two-dimensional version of the Goddard Cumulus Ensemble Model and their detailed model setup and physical schemes can be found in Gao and Li (2008). Large-scale forcing including vertical velocity and zonal wind (Figs. 1 and 2) was imposed in the model. PSRCO2 and COARECO2 are the corresponding sensitivity experiments to PSR and COARE. , They are identical to PSR and COARE, except that the magnitude of carbon dioxide in PSRCO2 and COARECO2 is twice as large as that in PSR and COARE.

Following Li et al. (1999), the model domain mean heat and specific humidity budgets can be expressed by

$$\frac{\partial \overline{T}}{\partial t} = \frac{\overline{Q}_{\rm cn}}{c_p} + \frac{\overline{Q}_{\rm R}}{c_p} - \frac{\pi}{\overline{\rho}}\frac{\partial(\overline{\rho}\overline{w'\theta'})}{\partial z} - \pi\overline{w}_{\rm o}\frac{\partial\overline{\theta}}{\partial z} - \pi\overline{u}_{\rm o}\frac{\partial\overline{T}_{\rm o}}{\partial z}\ . \quad (1)$$

Here T is temperature, θ is potential temperature; u and w are zonal and vertical components of winds; $Q_{\rm cn}$ is the net condensation, $Q_{\rm R}$ is radiation; $\pi = (p/p_0)^{R/c_p}$, R is gas constant, c_p is specific heat of dry air at constant pressure p, and $p = 1000$ hPa; ρ is height-dependent air density; Overbar is model domain mean, and prime is perturbation from domain mean, and subscript "o" is imposed value. The heat budget, Eq. (1), states that the local change of model domain mean temperature is determined by condensational heating ($\overline{Q}_{\rm cn}/c_p$), radiative heating ($\overline{Q}_{\rm R}/c_p$), convergence of vertical heat flux ($-\pi\partial(\overline{\rho}\overline{w'\theta'})/\overline{\rho}\partial z$), vertical temperature advection ($-\pi\overline{w}_{\rm o}\partial\overline{\theta}/\partial z$), and imposed horizontal temperature advection ($-\overline{u}_{\rm o}\partial\overline{T}_{\rm o}/\partial x$).

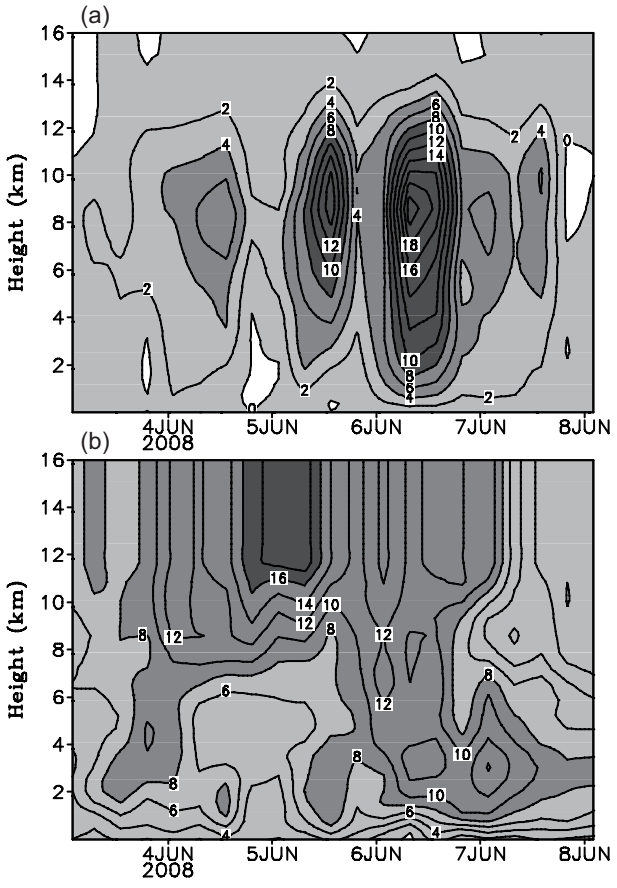

Fig. 1. Temporal and vertical distribution of (a) vertical velocity (cm s^{-1}) and (b) zonal wind (m s^{-1}) imposed in the experiments PSR and PSRCO2. Ascending motion in (a) and westerly wind in (b) are shaded. Reprinted from Shen et al. (2012b) by permission of copyright holders.

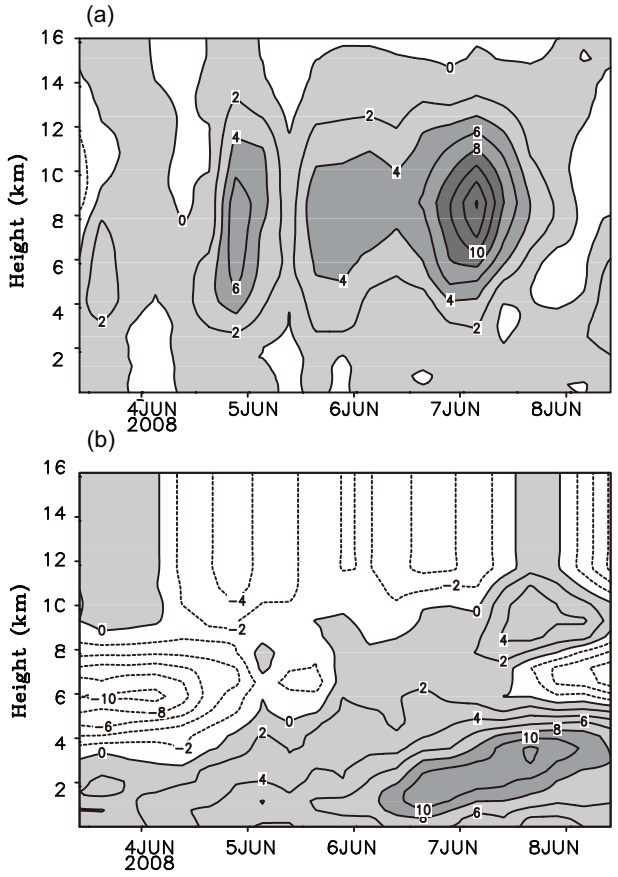

Fig. 2. Temporal and vertical distribution of (a) vertical velocity (cm s^{-1}) and (b) zonal wind (m s^{-1}) imposed in the experiments COARE and COARECO2. Ascending motion in (a) and westerly wind in (b) are shaded.

Based on Gao et al. (2005) and Cui and Li (2006), the surface rainfall budget can be written as

$$P_S = Q_{WVT} + Q_{WVF} + Q_{WVE} + Q_{CM} \, . \quad (2)$$

Here, P_S, Q_{WVT}, Q_{WVF}, Q_{WVE}, and Q_{CM} are surface rain rate, local water-vapor change, water vapor convergence, surface evaporation, and local hydrometeor change/hydrometeor convergence, respectively. The surface rainfall budget, Eq. (2) is derived through the combination of the water vapor budget,

$$Q_{WVT} + Q_{WVF} + Q_{WVE} = Q_{NC} \, , \quad (3)$$

and the cloud budget,

$$P_S = Q_{CM} + Q_{NC} \, . \quad (4)$$

Here, Q_{NC} is the net condensation (vapor condensation and deposition minus evaporation of precipitation hydrometeor). A partitioning scheme based on the surface rainfall budget proposed by Shen et al. (2010) is applied to grid-scale rainfall simulation data in this study and the data are separated into eight rainfall types: DCL, DCG, MCL, MCG, DDL, DDG, MDL, and MDG (see definitions of rainfall types in Table 1). Only seven of them are analyzed in this study because there was no rainfall of type MDG in either phase.

3. Results

3.1. *Model domain mean analysis*

The doubled carbon dioxide reduces the model domain mean surface rain rate from PSR to PSRCO2 (Table 2). The comparison in model domain mean cloud budgets between PSR and PSRCO2 shows that two-thirds and one-third of the reduced mean rain rate are associated with the weakened mean net condensation and decreased mean hydrometeor loss, respectively. Since the doubled carbon dioxide affects radiation and the change in latent heat corresponds to the change in net condensation, the model domain mean heat budgets are analyzed to explain the reduction in net condensation by doubled carbon dioxide. The differences in the time and model domain mean heat budget, Eq. (1), between PSRCO2 and PSR (PSRCO2 – PSR) in Fig. 3a show a reduced mean latent heat from 2 km to 5.5 km that is associated with the weakened mean net condensation. The reduced mean latent heat corresponds to the decreased mean infrared radiative cooling (Fig. 4a) in the thermal balance. The reductions in mean latent heat and infrared cooling are linked by the increase in the saturation mixing ratio and stable thermal stratification. The change in the saturation mixing ratio by the diurnal variation of radiation is a major factor that is responsible for the diurnal variation of the net condensation and rainfall (e.g., Tao et al., 1996; Gao and Li, 2010; Li and Gao, 2011). The stable thermal stratification is caused by the upward increase in magnitude of the weakened mean infrared radiative cooling. The weakened mean infrared radiative cooling between 13 km and the reduced mean solar radiative heating below 10 km are related to the doubled

Table 1. Summary of rainfall types. D and M represent local atmospheric drying and moistening, respectively. C and D represent water vapor convergence and divergence, respectively. L and G represent hydrometeor loss/convergence and gain/divergence, respectively.

Type	Description
DCL	Rainfall associated with local atmospheric drying, water vapor convergence, and hydrometeor loss/convergence
DCG	Rainfall associated with local atmospheric drying, water vapor convergence, and hydrometeor gain/divergence
MCL	Rainfall associated with local atmospheric moistening, water vapor convergence, and hydrometeor loss/convergence
MCG	Rainfall associated with local atmospheric moistening, water vapor convergence, and hydrometeor gain/divergence
DDL	Rainfall associated with local atmospheric drying, water vapor divergence, and hydrometeor loss/convergence
DDG	Rainfall associated with local atmospheric drying, water vapor divergence, and hydrometeor gain/divergence
MDL	Rainfall associated with local atmospheric moistening, water vapor divergence, and hydrometeor loss/convergence
MDG	Rainfall associated with local atmospheric moistening, water vapor divergence, and hydrometeor gain/divergence

carbon dioxide. The weakened mean latent heat above 2 km tends to destabilize the surface layer, which enhances the mean latent heat. The weakened mean latent heat from 2 km to 5.5 km is largely offset by the enhanced mean latent heat near the surface, which leads to the small reduction in mean net condensation shown in Table 2. The enhanced mean local atmospheric warming from 6 km to 14 km is primarily associated with the weakened mean infrared radiative cooling (Figs. 3a and 4a).

To generalize the rainfall responses to the doubled carbon dioxide, we carried out four additional pairs of sensitivity experiments during June and July 2008, the same period as PSR and PSRCO2. The integration periods were 0800 LST 10 June to 0800 LST 15 June 2008, 0800 LST 12 June to 0800 LST 17 June 2008, 0800 LST 24 June to 0800 LST 29 June 2008, and 0800 LST 6 July to 0800 LST 11 July 2008. Like PSR and PSRCO2, the four additional sets of sensitivity experiments show the decreases in the mean rain rate in response to the doubled carbon dioxide. The reduction in the mean rain rate is mainly associated with the weakened net condensation.

The doubled carbon dioxide increases the mean rain rate from COARE to COARECO2 (Table 2). The enhanced mean rainfall is associated with the strengthened mean net condensation. The analysis of the mean heat budgets (Fig. 3b) reveals an enhanced mean latent heat above 6 km and near the surface associated with the intensified mean net condensation. Note a large difference in heat budget between 3 km and 6 km in Fig. 3b. Such a large heat-budget difference may result from the vertical shift of heat divergence and latent heat in response to the large vertical wind shear (Fig. 2b) and the vertical shift of the melting level. This can be demonstrated by the similar averages of the heat budgets at these vertical levels in COARECO2 and COARE. The enhanced mean latent heat above 6 km corresponds to the strengthened mean infrared radiative cooling (Fig. 4b) through the reduced saturation mixing ratio and unstable thermal stratification. The increased mean latent heat corresponds to the weakened surface sensible heat. The strengthened mean local atmospheric warming above 6 km is associated with the enhanced mean latent heat that corresponds to the intensified mean infrared radiative cooling (Figs. 3b and 4b).

Table 2. Cloud budgets (P_S, Q_{NC}, and Q_{CM}) by the difference in P_S between experiments with current carbon dioxide concentration ($\boldsymbol{C}$) and doubled carbon dioxide (CCO2) averaged for 5 days over the model domain. $\boldsymbol{C}$ = (PSR, PSR1, PSR2, PSR3, PSR4, COARE). Units are mm h^{-1}. The integration period and area for constructing large-scale forcing are also included.

Integration period and area for constructing large-scale forcing	Experiment	P_S	Q_{NC}	Q_{CM}
0200 LST 3 June–0200 LST 8 June 2008; (21°–22°N, 108°–116°E)	PSR	1.36	1.33	0.03
	PSRCO2	1.33	1.31	0.02
0800 LST 10 June–0800 LST 15 June 2008; (24°–25°N, 107°–115°E)	PSR1	1.32	1.29	0.03
	PSR1CO2	1.29	1.27	0.02
0800 LST 16 June–0800 LST 19 June 2008; (21°–22°N, 108°–116°E)	PSR2	0.94	0.93	0.01
	PSR2CO2	0.92	0.90	0.02
0800 LST 24 June–0800 LST 29 June 2008; (21°–22°N, 108°–116°E)	PSR3	0.79	0.78	0.01
	PSR3CO2	0.77	0.75	0.02
0800 LST 6 July–0800 LST 11 July 2008; (22°–23°N, 110°–118°E)	PSR4	0.80	0.79	0.01
	PSR4CO2	0.78	0.76	0.02
1000 LST 19 December–1000 LST 24 December 1992; Intensive Flux Array	COARE	0.92	0.88	0.04
	COARECO2	0.95	0.92	0.03

3.2. *Partitioning analysis*

The net condensation is largely associated with water vapor convergence. Convective and stratiform rainfall corresponds to water vapor convergence and divergence, respectively. Convective–stratiform rainfall separation relies on magnitudes in radar reflectivity in observational studies (e.g., Churchill and Houze, 1984) or surface rain rate in numerical modeling (e.g., Tao et al., 1993). The partitioning analysis of

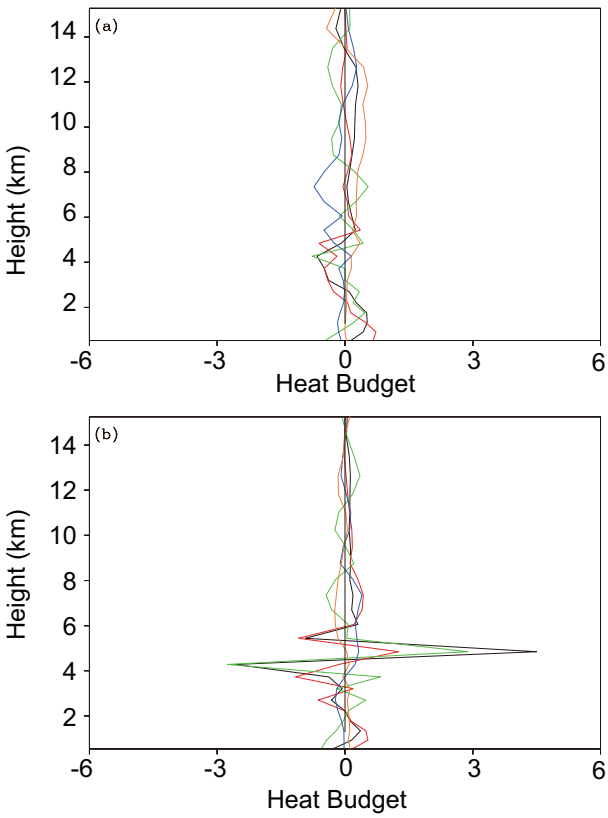

Fig. 3. Vertical profiles of differences between (a) PSRCO2 and PSR (PSRCO2 – PSR) and (b) COARECO2 and COARE (COARECO2 – COARE) for local temperature change (black), condensational heating (red), convergence of vertical heat flux (green), vertical temperature advection (blue), and radiation (orange) averaged for 5 days and model domain. Units are °C d^{-1}.

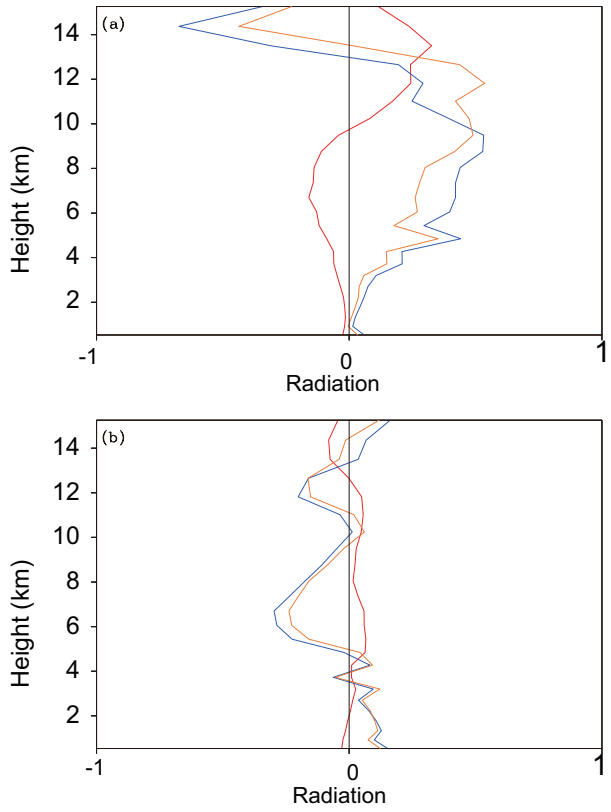

Fig. 4. The same as Fig. 3, except for radiation (orange) and its components: solar radiative heating (red) and infrared radiative cooling (blue).

convective–stratiform rainfall is compared with the analysis of the rainfall separation based on the surface rainfall budget, Eq. (2), developed by Shen et al. (2010) using COARE simulation data. The comparison study shows that a considerable portion of the convective rainfall is associated with water vapor divergence (Shen et al., 2012a). Thus, in this section we conduct a rainfall separation.

During the pre-summer torrential rainfall event, the doubled carbon dioxide increases the rainfall and the rainfall area of DDL from PSR to PSRCO2 (Table 3). The reduction in rainfall of DDL is associated with the decreases in local atmospheric drying and hydrometeor loss/convergence. The rainfalls of two other rain types associated with water vapor divergence (DDG and MDL) are lower than the rainfall of other rain types, and are generally insensitive to the change in carbon dioxide. For the four rain types associated with water vapor convergence, the rain rates of DCG, MCL, and MCG are higher than that of DCL, while the fractional coverage of DCG, MCL, and MCG is larger than that of DCL. The doubled carbon dioxide reduces the rainfall through the enhanced hydrometeor gain/divergence for DCG and the weakened water vapor convergence for MCG. The doubled carbon dioxide increases the rainfall of MCL via the suppressed local atmospheric moistening. The increased rainfall in MCL is offset by the weakened rainfall in DCG and MCG. These rain types have no contribution to the decrease in the mean

Table 3. (a) Fractional coverage and surface rainfall budget [(b) P_S, (c) Q_{WVT}, (d) Q_{WVF}, and (e) Q_{CM}] of seven rain types averaged for 5 days over the model domain in PSR, PSRCO2, COARE, and COARECO2. Surface evaporation (Q_{WVE}) is not shown because it is negligibly small compared to other terms in surface rainfall budget. Units are % for fractional coverage and mm h^{-1} for surface rainfall budget.

(a)	PSR	PSRCO2	COARE	COARECO2
DCL	0.35	0.37	0.17	0.16
DCG	1.81	1.81	1.11	1.51
MCL	7.44	6.88	7.16	9.30
MCG	5.21	4.74	4.65	5.55
DDL	11.86	10.60	9.67	11.62
DDG	2.60	2.31	2.29	3.34
MDL	1.27	1.29	1.02	1.23
(b)	PSR	PSRCO2	COARE	COARECO2
DCL	0.10	0.13	0.07	0.06
DCG	0.25	0.24	0.13	0.15
MCL	0.24	0.27	0.20	0.22
MCG	0.22	0.20	0.13	0.13
DDL	0.46	0.42	0.32	0.32
DDG	0.05	0.04	0.03	0.03
MDL	0.03	0.03	0.03	0.03
(c)	PSR	PSRCO2	COARE	COARECO2
DCL	0.03	0.04	0.02	0.02
DCG	0.20	0.20	0.11	0.14
MCL	−0.80	−0.71	−1.02	−1.14
MCG	−0.64	−0.56	−0.71	−0.72
DDL	1.38	1.23	1.55	1.61
DDG	0.34	0.25	0.38	0.44
MDL	−0.02	−0.03	−0.03	−0.02
(d)	PSR	PSRCO2	COARE	COARECO2
DCL	0.04	0.04	0.02	0.02
DCG	0.39	0.40	0.32	0.35
MCL	0.75	0.69	0.92	1.01
MCG	1.41	1.27	1.33	1.32
DDL	−1.57	−1.37	−1.80	−1.89
DDG	−0.20	−0.15	−0.28	−0.33
MDL	−0.03	−0.03	−0.03	−0.03
(e)	PSR	PSRCO2	COARE	COARECO2
DCL	0.03	0.05	0.03	0.02
DCG	−0.34	−0.37	−0.30	−0.35
MCL	0.29	0.28	0.28	0.32
MCG	−0.55	−0.51	−0.50	−0.48
DDL	0.64	0.55	0.54	0.56
DDG	−0.09	−0.07	−0.08	−0.09
MDL	0.08	0.08	0.09	0.08

rainfall. The doubled carbon dioxide increases the rain rate of DCL through the enhanced local atmospheric drying and the strengthened hydrometeor loss/convergence. The calculations of rain intensity with the rain rate divided by the fractional coverage reveal that PSRCO2 (35.1 mm h^{-1}) has a larger rain intensity than PSR (28.6 mm h^{-1}). Feng et al.

(2011) used a global AGCM to project future precipitation change over China under the A1B scenario (increased greenhouse gas emissions). They found that extreme precipitation increases significantly over southeastern China and that the percentage increase in extreme precipitation is larger than that of mean precipitation. The results here reveal that the increase in extreme rainfall is associated with the doubled carbon dioxide in the PSR case. The partitioning analysis of the PSR case shows that the reduction in the mean rain rate results from the decrease in the rainfall of DDL primarily through the weakened local atmospheric drying. The relationship between rainfall, local atmospheric drying, and infrared radiative cooling in the PSR case is similar to the diurnal rainfall theory developed by Gao and Li (2010) in which the enhanced nocturnal infrared radiative cooling leads to the nocturnal rainfall peak through weakened local atmospheric drying associated with the reduced saturation mixing ratio.

During COARE, the rainfall of DDL is insensitive to the change in carbon dioxide, while the rainfall area of DDL expands from COARE to COARECO2. The insensitivity of the rainfall of DDL is caused by the offset between the enhanced local atmospheric drying and strengthened water vapor divergence. Like PSR and PSRCO2, the doubled carbon dioxide barely changes the rainfalls of DDG and MDL during COARE. Among the four rain types associated with water vapor convergence, the doubled carbon dioxide barely changes the rainfall of MCG, increases the rainfalls of DCG and MCL, and slightly reduces the rainfall of DCL. The enhanced rainfall is associated with the increases in local atmospheric drying and water vapor convergence for DCG and water vapor convergence and hydrometeor loss/convergence for MCL. The weakened rainfall of DCL corresponds to the suppressed hydrometeor loss/convergence. Unlike those in the PSR case, the rain intensity decreases from COARE (41.2 mm h^{-1}) to COARECO2 (37.5 mm h^{-1}). The rainfall separation analysis suggests that the enhanced mean rain rate results from the increases in the rainfall of DCG and MCL.

4. Summary

The effects of carbon dioxide on rainfall responses to large-scale forcing were examined in this study. The two pairs of sensitivity experiments simulated pre-summer heavy rainfall over southern China around the summer solstice and tropical rainfall during TOGA COARE around the winter solstice using a two-dimensional cloud-resolving model. Each pair of sensitivity experiments included a control run and an additional simulation with doubled carbon dioxide. The major findings can be summarized as follows:

Doubled carbon dioxide enhanced atmospheric warming through the weakened infrared radiative cooling and enhanced solar radiative heating during the pre-summer torrential rainfall event around the summer solstice and latent heat during the tropical rainfall event around the winter solstice.

The reduced mean pre-summer rainfall caused by doubled carbon dioxide was primarily associated with the weakened mean net condensation during the summer solstice. The enhanced mean tropical rainfall resulting from doubled carbon dioxide was related to the strengthened mean net condensation during the winter solstice. The reduced mean net condensation corresponded to the weakened mean infrared radiative cooling through the strengthened saturation mixing ratio and stable thermal stratification during the pre-summer rainfall event and vice versa during the tropical rainfall event.

The weakened mean pre-summer rainfall resulted from the reduced rainfall associated with local atmospheric drying, water vapor divergence, and hydrometeor loss/convergence. The enhanced mean tropical rainfall was related to the strengthened rainfall from the rain type associated with local atmospheric drying, water vapor convergence, and hydrometeor gain/divergence and the rain type associated with local atmospheric moistening, water vapor convergence, and hydrometeor loss/convergence.

Care should be taken when applying the results of this study because the conclusions above were drawn from idealized 2D cloud-resolving model simulations. The results showed that the rainfall responses to doubled carbon dioxide depended on large-scale forcing, which was imposed on the model during the model integration. Thus, it is necessary to conduct further studies using three-dimensional interactive cloud-resolving model simulations to validate the results from 2D cloud modeling of rainfall responses to the increase in carbon dioxide.

Acknowledgements. The authors thank W.-K. TAO at NASA/GSFC for his cloud-resolving model and the three anonymous reviewers for their constructive comments. LI X. F. was supported by 985 Program of Zhejiang University under Grant No. 188020+193432602/215, National Natural Science Foundation of China (Grant No. 41175047), the R&D Special Fund for Public Welfare Industry by the Ministry of Finance and the Ministry of Science and Technology (Grant Nos. GYHY201006014 and 201005033-10) and the Basic Research Project of the State Key Laboratory of Severe Weather (12011LAS-B14). SHEN X. Y. and LIU J. were supported by the National Key Basic Research and Development Project of China under Grant Nos. 2013CB430103 and 2011CB403405, the National Natural Science Foundation of China under Grant Nos. 41375058 and 41175065.

REFERENCES

Bazzaz, F. A., 1990: The response of natural ecosystems to the rising global CO_2 levels. *Annual Review of Ecology and Systematics*, **21**, 167–196.

Chen, G. and I. M. Held, 2007: Phase speed spectra and the recent poleward shift of Southern Hemisphere surface westerlies. *Geophys. Res. Lett.*, **34**, L21805, doi: 10.1029/2007GL031200.

Churchill, D. D., and R. A. Houze Jr., 1984: Development and structure of winter monsoon cloud clusters on 10 December 1978. *J. Atmos. Sci.*, **41**, 933–960.

Cui, X. P., and X. F. Li, 2006: Role of surface evaporation in surface rainfall processes. *J. Geophys. Res.*, **111**, D17112, doi: 10.1029/2005JD006876.

Emori, S., and S. J. Brown, 2005: Dynamic and thermodynamic changes in mean and extreme precipitation under changed climate. *Geophys. Res. Lett.*, **32**, doi: 10.1029/2005GL023272.

Feng, L., T. J. Zhou, B. Wu, T. Li, and J.-J. Luo, 2011: Projection of future precipitation change over China with a high-resolution global atmospheric model. *Adv. Atmos. Sci.*, **28**, 464–476, doi: 10.1007/s00376-010-0016-1.

Fields, P. A., J. B. Graham, R. H. Rosenblatt, and G. N. Somero, 1993: Effects of expected global climate change on marine faunas. *Trends in Ecology and Evolution*, **8**, 361–367.

Folland, C. K., and Coauthors, 2001: Global temperature change and its uncertainties since 1861. *Geophys. Res. Lett.*, **28**, 2621–2624.

Gao, S. T., and X. F. Li, 2008: *Cloud-resolving Modeling of Convective Processes*. Springer, Dordrecht, 206 pp.

Gao, S. T., and X. F. Li, 2010: Precipitation equations and their applications to the analysis of diurnal variation of tropical oceanic rainfall. *J. Geophys. Res.*, **115**, D08204, doi: 10.1029/2009JD012452.

Gao, S. T., X. P. Cui, Y. S. Zhou, and X. F. Li, 2005: Surface rainfall processes as simulated in a cloudresolving model. *J. Geophys. Res.*, **110**, D10202, doi: 10.1029/2004JD005467.

IPCC, 2001: *Climate Change 2001: The Scientific Basis. Contribution of Working Group I to the Third Assessment Report of International Panel on Climate Change*, Houghton et al., Eds., Cambridge University Press, Cambridge and New York, 572 pp.

IPCC, 2007: *Climate Change 2007: Mitigation of Climate Change. Contribution of Working Group III to the Fourth Assessment Report of the Intergovernmental Panel on Climate Change*, B. Metz et al., Eds., Geneva, Switzerland, 852 pp.

Jones, P. D., and A. Moberg, 2003: Hemispheric and large-scale surface air temperature variations: An extensive revision and an update to 2001. *J. Climate*, **16**, 206–223.

Kharin, V. V., and F. W. Zwiers, 2005: Estimating extremes in transient climate change simulations. *J. Climate*, **18**, 1156–1173.

Li, H. M., L. Feng, and T. J. Zhou, 2011: Multi-model projection of July–August climate extreme changes over China under CO_2doubling. Part I: Precipitation. *Adv. Atmos. Sci.*, **28**, 433–447, doi: 10.1007/s00376-010-0013-4.

Li, X. F., and S. T. Gao, 2011: *Precipitation Modeling and Quantitative Analysis*. Springer Dordrecht, 240 pp.

Li, X. F., C.-H. Sui, K.-M. Lau, and M.-D. Chou, 1999: Large-scale forcing and cloud-radiation interaction in the tropical deep convective regime *J. Atmos. Sci*., **56**, 3028–3042.

Li, X. F, C.-H. Sui, and K.-M. Lau, 2002a: Interactions between tropical convection and its environment: An energetics analysis of a 2D cloud resolving simulation. *J. Atmos. Sci.*, **59**, 1712–1722.

Li, X. F., C.-H. Sui, and K.-M. Lau, 2002b: Dominant cloud microphysical processes in a tropical oceanic convective system: A 2-D cloud resolving modeling study. *Mon. Wea. Rev.*, **130**, 2481–2491.

Manabe, S., and R. T. Wetherald, 1975: The effects of doubling the CO_2 concentration on the climate of a general circulation model. *J. Atmos. Sci.*, **32**, 3–15.

Meehl, G. A., J. M. Arblaster, and C. Tebaldi, 2005: Understanding future patterns of increased precipitation intensity in climate model simulations. *Geophys. Res. Lett.*, **32**, doi: 10.1029/2005GL023680.

Shen, X. Y., Y. Wang, N. Zhang, and X. F. Li, 2010: Precipitation and cloud statistics in the deep tropical convective regime. *J. Geophys. Res.*, **115**, D24205, doi: 10.1029/2010JD014481.

Shen, X. Y., Y. Wang, and X. F. Li, 2011a: Radiative effects of water clouds on rainfall responses to the large-scale forcing during pre-summer heavy rainfall over southern China. *Atmospheric Research*, **99**, 120–128.

Shen, X. Y., Y. Wang, and X. F. Li, 2011b: Effects of vertical wind shear and cloud radiative processes on responses of rainfall to the large-scale forcing during pre-summer heavy rainfall over southern China. *Quart. J. Roy. Meteor. Soc.*, **137**, 236–249.

Shen, X. Y., N. Zhang, and X. F. Li, 2011c: Effects of large-scale forcing and ice clouds on pre-summer heavy rainfall over southern China in June 2008: A partitioning analysis based on surface rainfall budget. *Atmospheric Research*, **101**, 155–163.

Shen, X. Y., J. Liu, and X. F. Li, 2012a: Evaluation of convective-stratiform rainfall separation schemes by precipitation and cloud statistics. *Journal of Tropical Meteorology*, **18**, 98–107.

Shen, X., J. Liu, and X. Li, 2012b: Torrential rainfall responses to ice microphysical processes during pre-summer heavy rainfall over southern China. *Adv. Atmos. Sci.*, **29**, 493–500, doi: 10.1007/s00376-011-1122-4.

Tao, W.-K., J. Simpson, C.-H. Sui, B. Ferrier, S. Lang, J. Scala, M.-D. Chou and K. Pickering, 1993: Heating, moisture and water budgets of tropical and midlatitude squall lines: Comparisons and sensitivity to longwave radiation. *J. Atmos. Sci.*, **50**, 673–690.

Tao, W.-K., S. Lang, J. Simpson, C.-H. Sui, B. Ferrier, and M.-D. Chou, 1996: Mechanisms of cloud-radiation interaction in the tropics and midlatitudes. *J. Atmos. Sci.*, **53**, 2624–2651.

Tebaldi, C., K. Hayhoe, J. M. Arblaster, and G. A. Meehl, 2006: Going to the extremes: An intercomparison of model-simulated historical and future changes in extreme events. *Climatic Change*, **79**, 185–211.

Vecchi, G. A. and B. J. Soden, 2007: Global warming and the weakening of the tropical circulation. *J. Climate*, **20**, 4316–4340.

Wang, Y., X. Y. Shen, and X. F. Li, 2010: Microphysical and radiative effects of ice clouds on responses of rainfall to the large-scale forcing during pre-summer heavy rainfall over southern China. *Atmospheric Research*, **97**, 35–46.

Weller, R. A., and S. P. Anderson, 1996: Surface meteorology and air-sea fluxes in the western equatorial Pacific warm pool during the TOGA Coupled Ocean Atmosphere Response Experiment. *J. Climate*, **9**, 1959–1990.

Wu, Y. T., R. Seager, M. F. Ting, N. Naik, and T. A. Shaw, 2012: Atmospheric circulation response to an instantaneous doubling of carbon dioxide. Part I: Model experiments and transient thermal response in the troposphere. *J. Climate*, **8**, 2862–2879.